A Biomimetic Non-antibiotic Approach to Eradicate Drug-resistant Infections

Yu Zhao,[a] Qianqian Guo,[a] Xiaomei Dai,[a] Xiaosong Wei,[a] Yunjian Yu,[a] Xuelei Chen,[a] Chaoxing Li,[a] Zhiqiang Cao,[b,*] Xinge Zhang [a,*]

[a] Key Laboratory of Functional Polymer Materials of Ministry Education, Institute of Polymer Chemistry, College of Chemistry, Nankai University, Tianjin 300071, China

[b] Department of Chemical Engineering and Materials Science, Wayne State University, Detroit, Michigan 48202, USA

[*] Corresponding author.

E-mail: zhangxinge@nankai.edu.cn;

zcao@wayne.edu

Keywords

biofilm inhibition, anti-adhesion, heteromultivalency, subcutaneous abscesses, pneumonia, photothermal therapy

Abstract

The chronic infections by pathogens such as *Pseudomonas aeruginosa* (*P. aeruginosa*) and other related bacteria remained to be properly addressed. In particular, for drug-resistance strains, limited medication was available. We developed an *in vivo* pneumonia model induced by a clinically isolated aminoglycoside-resistant strain of *P. aeruginosa*. Tobramycin, antibiotics clinically used to treat *P. aeruginosa* infections was found to be ineffective to inhibit or eliminate this particular drug-resistant strain. We showed that a newly developed non-antibiotics based nano-formulation plus near-infrared (NIR) photothermal treatment showed a remarkable antibacterial efficacy in treating this drug-resistant pneumonia. The novel formulation contained 50-100 nm long nanorods decorated with two types of glycomimetic polymers to specifically block LecA and LecB lectins, respectively, which are essential for biofilm development of *P. aeruginosa.* Such heteromultivalent presentation of glycomimetics and their 3-dimensional (3-D) display on a large scale is inspired by the natural strengthening mechanism for carbohydrate-lectin interaction occurred when bacteria initially infect the host. This biomimetic anti-adhesion strategy has rarely been reported before. This novel formulation showed the most efficient bacteria inhabitation and killing against *P. aeruginosa* infection: It inhibited bacterial adhesion to epithelial cells, and biofilm inhibition capacity was up to 90%. Additionally, the gold nanorods were able to convert near-infrared light to heat, resulting in the bacterial cell death and further elimination of the bacteria. Collectively, we expect the novel biomimetic design combined with the photothermal killing capability to be the next generation antimicrobial agents against *P. aeruginosa*, and potentially other

infections, and as alternative treatment strategy against the ever-threatening drug-resistant infectious diseases when known antibiotics failed.

Pseudomonas aeruginosa is a gram-negative opportunistic microorganism contributing to 10-20% of nosocomial infections worldwide. It typically infects patients, such as those with a respiratory infection, urinary tract infection, gastrointestinal infection, keratitis, otitis media, and bacteremia.[1] Commonly used antibacterial or antibiotic agents for eliminating *P. aeruginosa* infections include *β*-lactams, aminoglycosides and fluoroquinolones.[2] Polymyxins have been used for this purpose too, but only for treating multidrug-resistant strains due to their high toxicity.[3] Certain antibiotic drug combinations have shown improved performance in treating *P. aeruginosa*.[2c,4] Nevertheless, *P. aeruginosa* is inherently resistant to conventional antibiotic agents, due to the low permeability of the bacterial membrane and the increased efflux of the drugs.[5] This leads to multiple treatment complications, treatment failure, and even death. Therefore it is urgent to develop a non-antibiotic based strategy against *P. aeruginosa*.

Infection by pathogens is generally triggered by crucial steps of recognition and adhesion on host epithelial surfaces. Efficient bacterial adhesion facilitates the pathogens to escape from the host's natural cleansing mechanism and eventually results in forming biofilms.[6] It is well known that micro-organisms such as bacteria used lectin, a carbohydrate-binding protein, to specifically interact with glycans on host tissues. LecA from *P. aeruginosa* is a lectin specifically targeting galactose, and is essential for the bacterium internalizing to the cells.[7] LecB from *P. aeruginosa* can strongly bind fucose and fucose-containing oligosaccharides, contributing to the bacterial adhesion to the airway epithelial cells.[8] The biofilm formation by *P.*

aeruginosa has been shown to be mediated by LecA and LecB in *in vitro* and *in vivo* studies.[9] These two lectins are therefore interesting targets for the prevention of bacterial colonization and potential biofilm formation.[10]

Individual interactions between proteins and carbohydrates are usually feeble, and this deficiency is often addressed by heteromultivalency on both the glycan and the lectin sides in living systems.[11] When the bacteria come into contact with the host cells during the initial phase of an infection, multiple types of carbohydrate moieties on the cell surfaces bind different types of lectins on bacteria within a large scale (from nm to μm) 3-D contacting area.[12] Such heteromultivalent and large-scale 3-D presentation of carbohydrate-protein interaction is critical for the biofilm development and stabilization, however, has rarely been considered in designing current bacterial inhibitory agents.[9a,13] Majority bacterial inhibitory glycomimetics studied so far are homomultivalent, e.g. they contained only one single type of sugar residue,[14] or presented within a small 3-D area below a few nanometers, e.g., glycomimetics were displayed on dendrimers.[15]

In the present study, we developed a versatile platform for constructing heteromultivalent carbohydrates-functionalized 3-D nanostructures by conjugating glycomimetics-based galactose and fucose ligands to target two key lectins on *P. aeruginosa*, and presenting them on gold nanorods of 50-100 nm in length. The resulting novel formulation was found to agglutinate *P. aeruginosa* much more effectively than the parent water-soluble carbohydrates or the counterparts containing only single carbohydrate. The nanoconjugates exhibited faster adhesion rate and

lower effective concentration than the reported materials.[16] More importantly, the biomimetic design of this formulation enabled so far the best inhibition of bacterial adhesion and biofilm formation by *P. aeruginosa* compared to reported inhibitory studies.[9a,17]

An inhibitory agent was able to prevent bacterial adhesion on cells and biofilm formation but typically cannot kill the pathogens. As an additional benefit, the nanoconjugate formulation contained gold nanorods (AuNRs), which have shown the photothermal property to kill pathogenic cells upon near-infrared (NIR) light irradiation.[18] It should be noted that NIR light within 650 – 900 nm are favorable for *in vivo* application because of minimum photo-damage to biological samples, deep tissue penetration, and minimum interference from background auto-fluorescence by biomolecules in the living systems.[19] In an *in vitro* study, we showed that the nanoconjugate agent was able to kill nearly 100% bacteria within 3 min under the NIR irradiation, by destroying bacteria cell membranes. With combined inhibitory and photothermal functions of the nanoconjugates, we further showed an outstanding antibacterial performance and an accelerated host recovery in subcutaneous abscesses and pneumonia induced by a clinically isolated, aminoglycoside-resistant strain of *P. aeruginosa*. The healed sites did not show any observable inflammation, with the expressed inflammatory marker level as low as a healthy tissue.

The synthesis of pLAMA (to bind LecA) and pFEMA (to bind LecB) was carried out by RAFT (**Scheme S**1, Supporting Information). The ^{1}H NMR of pLAMA and pFEMA with a uniform distribution of molecular weight was shown in **Figure S**1 and

Table S1, Supporting Information. AuNRs stabilized by thiol-terminated carbohydrate polymers were prepared from hexadecyl trimethyl ammonium bromide (CTAB)-stabilized NRs based on the previous method.[20] AuNRs were functionalized with pLAMA and pFEMA and showed excellent stability in water (**Figure 1**a). The morphology of the nanoconjugate formulations was observed by TEM (**Figure 1**b). AuNRs@glycomimetics with a rod-like shape was approximately 50-100 nm in size and had an aspect ratio of 7.0-8.3 (**Table S**2, Supporting Information), and showed good dispersibility in water. AuNRs@glycomimetics were named AuNRs@pLAMA/pFEMA which represented AuNRs decorated with pLAMA and pFEMA. The marked number for AuNRs@pLAMA/pFEMA was used to distinguish the polymerization degree. UV-vis-NIR spectra (**Figure 1**c) demonstrated that the absorption peaks of AuNRs and AuNRs@glycomimetics were 859 and 872 nm, respectively. Compared to AuNRs, AuNRs stabilized with glycomimetics caused a red shift of absorption, indicating that thiol groups at the polymer chain end bonded to the gold surface. Simultaneously, we used the sulfuric acid-phenol method to determine the polymeric content in the nanoconjugates,[21] and found that there was approximately an average of 5500 glycomimetic chains conjugated on the surface of each AuNR.

Upon irradiation with a NIR laser (808 nm, 2 W/cm^2), temperature changes were observed in the aqueous solution containing the nanoconjugates at varying concentrations (0, 125, 250, 500 and 1000 μg/mL) (**Figure 1**d). As expected, the NIR-irradiated nanoconjugates rapidly released heat as a function of laser exposure

time. An obvious effect of concentration-dependent temperature increase was clearly observed. At a concentration as low as 125 μg/mL, the NIR light over a period of 5 min induced a temperature increase in the nanoconjugates aqueous solution from 27.1 to 42.5 °C. The efficient conversion of laser energy to thermal energy is attributed to the strong localized surface plasmon resonance of AuNRs in the NIR region, which is known to lead to good photothermal properties.[22]

Multivalent glycocompounds have shown to interfere with lectin-mediated pathogen adhesion.[15a] *P. aeruginosa* was used to evaluate potential binding between glycomimetics functionalized AuNRs and *P. aeruginosa*. Since photoluminescence of AuNRs could be observed following laser excitation, binding of the nanoconjugates to bacteria was imaged microscopically. The bacteria presented dispersion state after co-cultured with naked AuNRs (**Figure S**2, Supporting Information) while it was found that a great number of *P. aeruginosa* cells bound to the fluorescent AuNR@pLAMA/pFEMA and formed clusters (**Figure 2**a). The larger clusters had stronger fluorescence signal, while single cells in the culture exhibited weak fluorescence. To confirm that AuNRs@pLAMA/pFEMA specifically bind *P. aeruginosa*, we co-cultured the nanoconjugates with *E. coli*. As shown in **Figure 2**a, *E. coli* remained as individual cells and did not form aggregations.

Compared with individual pLAMA or pFEMA functionalized AuNRs, AuNRs@pLAMA/pFEMA exhibited the largest bacterial clusters, especially AuNRs@pLAMA/pFEMA-50 (**Figure 2**a), indicating that there was a synergistic effect between galactose and fucose glycomimetics to capture LecA and LecB, which

play a prominent role in human infections. The degree of polymerization (DP) of the glycomimetics significantly influenced the adhesion capacity of the nanoconjugates. More sugar moieties in the polymer chain are expected to enhance the affinity of the nanoconjugates to LecA and LecB lectins. Nevertheless, long polymer chain (such as DP = 70 glycomimetics) might not fully stretch in water and presented in the coiled state, reducing the binding capability of nanoconjugates to bacteria.

To determine the minimum concentration of the nanoconjugate-bound *P. aeruginosa*, we tested the OD_{600} value of bacteria incubated with the nanoconjugate at different concentrations for 1 h (**Figure 2**b). Potential bacteria binding to the nanoconjugates led to bacteria aggregation and precipitation, resulting in a lowered OD_{600} value. When the concentration of all tested nanoconjugates was 15.6 μg/mL, the adhesion capacity, the percentage of bacteria adhered and precipitated, was up to 50%, which was much more than AuNRs with the same concentration. When the concentration was as low as 3.9 μg/mL, the adhesion capacity still reached 38%. Long-chain glycomimetics (such as DP = 50, 70) may not be fully stretched at high concentration. This reduced the effective sugar content binding to lectins, as was observed that AuNRs@pLAMA/pFEMA-50 and AuNRs@pLAMA/pFEMA-70 displayed relatively poor adhesion performance to *P. aeruginosa* compared with AuNRs@pLAMA/pFEMA-30.

We further tested the rate of bacterium-nanoconjugate binding at a constant nanoconjugate concentration of 500 μg/mL within 80 min (**Figure 2**c). It was found that AuNRs@pLAMA/pFEMA-30 bound bacteria significantly faster than

AuNRs@pLAMA/pFEMA-50 and AuNRs@pLAMA/pFEMA-70, consistent with the results in **Figure 2**b. For AuNRs@pLAMA/pFEMA-30, it only took 50 min to reach 50% adhesion capacity (50% reduction of OD_{600} value).

The formation of a biofilm plays an important role in antibiotic resistance and disease progression.[9b] Biofilm formation by *P. aeruginosa* is mediated, in part, by the galactose-specific lectin LecA and the fucose-specific lectin LecB,[8b,23] as shown by studies using deletion mutants and the partial inhibitory effect of simple fucose and galactose derivatives *in vitro* and *in vivo*.[9a,24] We measured the inhibition of biofilm formation at different concentrations of the nanoconjugates (**Figure 3**a). The concentration being able to inhibit 50% biofilm formation was defined as $MBIC_{50}$. The amount of biofilm formed for the untreated group was defined as 100%. It was found that the $MBIC_{50}$ of AuNRs@pLAMA/pFEMA-30, AuNRs@pLAMA/pFEMA-50, and AuNRs@pLAMA/pFEMA-70 was approximately 58, 12.5, and 75 μg/mL, respectively, indicating that AuNRs@pLAMA/pFEMA-50 showed the most significant biofilm inhibition among the three AuNRs@glycomimetics.

To evaluate the effect of different glycomimetic types on the biofilm inhibition, the relative capacity of biofilm inhibition was further carried out after treatment with AuNRs@pLAMA-50, AuNRs@pFEMA-50, and AuNRs@pLAMA/pFEMA-50, respectively (**Figure 3**b). The inhibition rate of AuNRs@pLAMA-50 and AuNRs@pFEMA-50 containing a single type of glycomimetic ligand was found to be 72% and 78%, while the rate for AuNRs@pLAMA/pFEMA-50 containing two types

of ligands simultaneously reached 90% at 800 μg/mL. Such boosted synergistic effect on biofilm inhibition was attributed to the excellent bacterial binding capability of this nanostructure.

The effect of the glycomimetic length on biofilm inhibition was examined by confocal laser scanning microscope (CLSM) (**Figure 4**a). The biofilm polysaccharide was stained with FITC-labeled Concanavalin A (ConA-FITC) showing green fluorescence. *P. aeruginosa* was stained with ethidium bromide (EB) showing red florescence. The untreated biofilm control was dense and formed a whole piece. On the contrast, the treated groups showed bacterial cells and polysaccharides of much less amount and highly scatteredly distributed. AuNRs@pLAMA/pFEMA-50 continuously stood out by showing the greatest inhibition efficiency, compared with counterparts with different glycomimetic polymer lengths. The effect of glycomimetic ligand types on biofilm inhibition was also explored (**Figure 4**b). Similar to the results in **Figure 3**b, AuNRs@pLAMA/pFEMA-50 containing two types of ligand showed significantly enhanced synergistic effect to inhibit biofilm formation, compared with AuNRs@pLAMA-50 and AuNRs@pFEMA-50 containing only one ligand.

Since carbohydrates could inhibit bacterial adhesion, the capability of glycomimetics-decorated gold nanorods to prevent the binding or contact of *P. aeruginosa* to host cells was examined. A549 epithelial cells were incubated with *P. aeruginosa* to simulate an infection process, and then vigorously washed to eliminate non-adhering bacterial cells and subsequently incubated with PBS for 2 h. No detachment of bacterial cells was observed in this untreated group, and a significant

amount of bacterial cells were found to adhere to the cell membranes (**Figure 5**a). When treated with 100 μg/mL of the most potent nanoconjugate, AuNRs@pLAMA/pFEMA-50, after the bacterial-cell incubation, the majority of bacterial cells were washed out showing the drastically reduced amount of adhered bacteria on the cells. This finding suggested that the nanoconjugates disrupted the established interaction between A549 epithelial cells and *P. aeruginosa*. The inhibition effect of AuNRs@pLAMA/pFEMA-50 was significantly better than the untreated PBS and AuNRs control, and AuNRs@pLAMA-50 and AuNRs@pFEMA-50 containing only one type of ligand, indicating the necessity for heteromultivalency to achieve a synergistic effect (**Figure 5**a).

To quantify the number of bacteria adhered to the cells either with or without nanoconjugate treatment, we used LB agar plates to determine the number of Colony-Forming Units (CFU). The addition of AuNRs@pLAMA-50 and AuNRs@pFEMA-50 (containing one type of ligand) resulted in approximately 60% of *P. aeruginosa* adhered on cells compared with 100% for the untreated control group (**Figure 5**b). AuNRs@pLAMA/pFEMA-50 (containing two types of ligand showing the synergistic effect) exhibited far better inhibition capability resulting in less than 30% bacteria remained on cell surfaces. These results in **Figure 5**a and **5**b demonstrated that pLAMA and pFEMA chains were able to disrupt established interactions between epithelial cell ligands and bacterial lectin adhesion domains.

The toxicity of the nanoconjugates to A549 (**Figure 5**c) and NIH3T3 cells (**Figure S**3, Supporting Information) was evaluated using the MTT assay. Cells were treated with

the nanoconjugates at different concentrations (from 15.6 to 500 μg/mL) for 24 h. Then the cell viability was examined and found to be greater than 80% at concentrations ≤ 62.5 μg/mL of all nanoconjugates tested. This indicates low toxicity of nanoconjugates to A549 cells. Hemolysis assay of AuNRs@pLAMA/pFEMA treated with red blood cells showed that the nanoconjugates with good biocompatibility (**Figure S**3, Supporting Information).

To examine bactericidal efficacy resulted from photothermal treatment of the nanoconjugates, we used a live/dead assay to characterize cell survival of *P. aeruginosa* by acridine orange (AO) staining (green; label live cells) and EB staining (red; label dead cells). When bacterial cells were co-cultured with the nanoconjugates in the dark environment, all cells showed green, indicating that the bacteria were not killed by AuNRs@pLAMA/pFEMA (**Figure 6**a). After 2 min NIR laser irradiation, all bacterial cells treated with nanoconjugates showed red, suggesting the photothermal function of the agents and their rapid and efficient bactericidal effect. We further used LB agar culture to grow colonies and quantify the number of survived bacterial cells after different irradiation periods of time (**Figure S**4, Supporting Information). Longer irradiation time generally decreased the number of colonies, and for all tested nanoconjugates, only 3 min was needed to completely kill the bacteria (nearly zero colonies on the plate).

P. aeruginosa cells treated by AuNRs@pLAMA/pFEMA-50 either with or without NIR exposure were observed under the scanning electron microscopy (SEM) (**Figure 6**b). Without NIR laser irradiation, the bacterial cell surface showed integral and

smooth membrane structures, similar to native live bacterial cells without treatment of nanoconjugates. After 3 min of NIR exposure, bacterial cells treated with nanoconjugates showed severely damaged and ruptured cell membranes. We expect the efficient bactericidal effect results from the rupture of cell membrane through the NIR induced localized overheating. It should be noted that without treatment of nanoconjugate, NIR exposure alone did not kill the bacteria and no damage to the cell membrane can be observed (**Figure 6**b).

To evaluate the *in vivo* therapeutic performance of the novel antibacterial nanoconjugate formulations, we used *P. aeruginosa* to infect BALB/c mice to generate a subcutaneous abscesses model (**Figure 7**a), As AuNRs@glycomimetics did not trigger hemolysis and showed low toxicity to NIH3T3 cells (**Figure S**3, Supporting Information), we injected AuNRs@pLAMA/pFEMA-50 into the abscesses area directly and after applying 808 nm NIR irradiation, the temperature of abscess site increased up to 60 °C rapidly as recorded by the IR thermal camera (**Figure 7**b). The NIR treatment was conducted for 5 min at specified intervals and after 9 days treatment, the abscess tissues were excised and homogenized, and the numbers of CFU of bacteria were calculated by standard plate counting methods. The number of CFU in each treatment group was normalized by using the CFU of the experimental group divided by the CFU of the control group (PBS injection without NIR treatment). The CFU counts in the group treated with AuNRs@pLAMA/pFEMA-50 under 808 nm NIR irradiation were significantly lower than other groups without application of the nanoconjugates, NIR irradiation, or both,

indicating that the novel nanoconjugate plus photothermal therapy was able to eliminate the majority of bacteria from the tissue (**Figure 7**c). To visually monitor the therapeutic effect, we took pictures of the skin conditions from 0 to 9 days after the nanoconjugate treatment (**Figure 7**d). The skin treated with AuNRs@pLAMA/pFEMA-50 under NIR irradiation presented commendable wound repairing only within 3 days treatment by forming a scab. After 9 days treatment, the AuNRs@pLAMA/pFEMA-50 under NIR irradiation group had the scab fallen off and displayed complete healing, whereas for control group without a treatment, the skin around the scab remained erythematous and inflamed.

Histological evaluation of the abscess provided insight into the impact of photothermal therapy. Hematoxylin-eosin staining on skin sections showed severe infection on tissues before any nanoconjugate based treatment (**Figure 8**a). After 9-day treatment with AuNRs@pLAMA/pFEMA-50 plus NIR irradiation, there was an obvious reduction of the infiltrated inflammatory cells, indicating a remarkable bactericidal effect and high biocompatibility of the nanoconjugate.

In all mammals, a heat-shock response, induced by a wide range of stimuli, increases the expression of a family of proteins called heat-shock proteins (HSPs).[25] HSPs act as molecular chaperones for cells under stress and exhibit cytoprotective properties.[26] We further analyzed the expression of the BAG3 protein, a member of heat shock protein co-chaperones and whose expression is regulated by HSPs in response to hyperthermia and other environmental stresses.[27] Immunohistochemical staining results indicated that tissues treated with AuNRs@pLAMA/pFEMA-50 upon NIR

stimulation showed a significantly enhanced expression of BAG3 compared with non-stimulated groups (**Figure 8**a and **8**b). This implied that heat generated by AuNRs@pLAMA/pFEMA-50 could stimulate the encoding of BAG3, preventing normal tissues from heat injuries.

Additionally, we analyzed the expression of tumor necrosis factor alpha (TNF-α), an essential indicator characterizing the host inflammatory response.[28] Wounds treated with AuNRs@pLAMA/pFEMA-50 under 808 nm NIR irradiation exhibited the lowest expression level of TNF-α, similar to a healthy tissue, compared with other experimental and control groups (**Figure 8**a and **8**c). This indicated almost no inflammatory response after 9 days of treatment.

We further tested the antibacterial efficacy of the nanoconjugate against a clinically isolated strain of aminoglycoside-resistant *P. aeruginosa*. Tobramycin (1 mg/mL), a clinically used treatment to *P. aeruginosa* infection, was co-cultured with the aminoglycoside-resistant *P. aeruginosa* (10^8 CFU/mL) for 6 hours, and was found to be inefficient to inhibit or eliminate the resistant strain in the live/dead assay under CLSM (**Figure S**5, Supporting Information). The nanoconjugate with merely 3 min irradiation was found to reliably and effectively kill the aminoglycoside-resistant *P. aeruginosa*.

As *P. aeruginosa* is a major cause of chronic lower respiratory tract infections, we developed an *in vivo* pneumonia model in mice using the aminoglycoside-resistant *P. aeruginosa* according to the previously reported method.[29] After pulmonary administration of the bacteria, mice had shown breathing difficulty, weight loss, and

activity reduction—an indication of the establishment of pneumonia. Anatomy results indicated local lung necrosis of this model. The nano-formulation was pulmonary administered. After 5-day treatment, the lung was excised and homogenized and the CFU number of bacteria in each group was obtained (**Figure 9**a). Remarkably, the AuNRs@pLAMA/pFEMA-50 under NIR irradiation showed the lowest CFU level in the lung compared with other groups ($p < 0.05$), indicating an effective removal of the bacteria from the lung.

P. aeruginosa lung infection is characterized by acute pulmonary inflammation, high levels of cytokine and chemokine production and massive recruitment of neutrophils. Bacterial infection generally initiates an immune response, resulting in an increase of inflammatory cytokines. Therefore, the capability of this nano-formulation to regulate the immune response in the lung was evaluated following bacterial infection by quantifying inflammatory cells and inflammatory cytokines obtained from bronchoalveolar lavage fluid (BALF).[30] As shown in **Figure 9**b, the number of neutrophils, macrophages and lymphocytes in the lung tended to increase after *P. aeruginosa* infection. The levels of these immune cells were down-regulated by AuNRs@pLAMA/pFEMA-50 under NIR irradiation to a level similar to the healthy group, compared with other experimental and control groups. Bacterial pneumonia is known for causing inflammatory reactions,[31] and consequently, the amount of total protein might increase in the lung tissue as transudation or exudation.[32] As shown in **Figure 9**c, the amount of total protein in treatment groups increased significantly compared with the healthy group, but AuNRs@pLAMA/pFEMA-50 under NIR

irradiation presented the lowest level among other treatment groups with statistical significance ($p < 0.05$). A large number of pro-inflammatory cytokines, including IL-1β, IL-6 and TNF-α, play a critical role in the initiation and development of inflammatory disease.[33] As shown in **Figure 9**d, **9**e, and **9**f, the levels of IL-1β, IL-6 and TNF-α in the lung BALFs in the AuNRs@pLAMA/pFEMA-50 under NIR irradiation group were significantly decreased compared with the other treatment groups. AuNRs@pLAMA/pFEMA-50 under NIR irradiation treatment is likely to attenuate pneumonia-associated lung inflammation by suppressing the release of proinflammatory cytokines, reduces the signals attracting neutrophils to the lungs.

We further examined bacterial loads in the lung area by immunofluorescence with a specific antibody against *P. aeruginosa*, where lung cells were stained with DAPI (blue fluorescence) and *P. aeruginosa* was stained with Cy3 (red fluorescence). Severe bacterial infection was confirmed before the treatment. Lungs treated with PBS, PBS plus NIR and AuNRs@pLAMA/pFEMA-50 contained significant bacteria, while the bronchial cavity of the mice treated with AuNRs@pLAMA/pFEMA-50 under NIR irradiation had almost no bacteria in presence (**Figure 10**). Histopathological analyses indicated that the lung alveoli of PBS or AuNRs@pLAMA/pFEMA-50 treated mice were severely damaged, with abundant inflammatory cells infiltrated comparing with the healthy group (**Figure 10**). It was noteworthy that the lungs appeared to have reduced damage after treated with AuNRs@pLAMA/pFEMA-50 under NIR irradiation and the integrity of the alveoli was significantly better than the other infected groups. When challenged with *P.*

aeruginosa, airway epithelial cells typically show increased activation of the nuclear transcription factor-kappa B (NF-κB), which leads to overproduction of proinflammatory cytokines IL-6 and 8, and TNF-α.[34] NF-κB p65 is a subunit of NF-κB, and bacterial pneumonia markedly promoted NF-κB p65 expression.[35] We used immunofluorescence method to observe the expression of NF-κB p65, where the lung cells were stained with DAPI (blue fluorescence) and NF-κB p65 was stained with Alexa Fluor 488 (green fluorescence). As shown in **Figure 10**, the lung immunohistochemical and immunofluorescence results indicated that AuNRs@pLAMA/pFEMA-50 under NIR irradiation significantly reduced the expression of NF-κB p65, while other groups still remained with bacterial-pneumonia infection.

Here we developed a novel antibacterial nanoconjugate formulation showing the most efficient biofilm inhibition (capacity up to 90%) and bacteria killing (nearly 100%) against *P. aeruginosa* infection. The outstanding bacterial inhibitory effect was attributed to heteromultivalent and 3-D display of two types of glycomimetic polymers on 50-100 nm scale nanostructures to specifically target LecA and LecB lectins on *P. aeruginosa*. This is a novel blocking approach mimicking the natural strengthening mechanism for carbohydrate-lectin interaction but has never been achieved before. The outstanding bacteria-killing effect was attributed to the capability of gold nanorods in converting near-infrared light to heat, resulting in the bacterial cell death and further elimination of the bacteria, facilitating the recovery of the host from severe inflammation induced by a clinically isolated strain of

drug-resistant *P. aeruginosa*. The design strategy can be utilized to further generate antibacterial agents for the efficient treatment of other infections as well.

Supporting Information

Supporting Information is available from the Wiley Online Library or from the author.

P. aeruginosa strains, cells, antibodies, and other reagents used in this study are described in Supporting Information. Detailed information on the synthesis and characteristics of materials, hemolysis and cytotoxicity assays, anti-adhesion property, in vivo anti-infection experiments, antibody staining, leukocyte, total protein, IL-1β, IL-6 and TNF-α assays, histological analysis, and statistics can be found in Supporting Information. This study was performed according to protocols approved by the University of Science and Technology of China Animal Care and Use Committee.

Acknowledgments

We are grateful to Dr. Haijin Xu and Professor Mingqiang Qiao (College of Life Sciences, Nankai University) for valuable discussion. This work was supported by the National Natural Science Foundation of China (grant No. 21474055 and 21774062 to X.Z.; 51673102 to C.L.), the Natural Science Foundation of Tianjin, China (grant No. 18JCYBJC29300 to X.Z.), US National Science Foundation (grant No. DMR-1410853 and DMR- 1809229 to Z.C.) and the US National Institute of Diabetes And Digestive And Kidney Diseases of the National Institutes of Health (grant Mo. DP2DK111910 to Z.C.).

Conflict of Interests

The authors declare no conflict of interest.

Keywords

biofilm inhibition, anti-adhesion, heteromultivalency, subcutaneous abscesses, pneumonia, photothermal therapy

References

[1] P. Roussel, G. Lamblin, *Adv. Exp. Med. Biol.* **2003**, *535*, 17.

[2] a) D. M. Livermore, *Clin. Infect. Dis.* **2002**, *34*, 634; b) E. B. M. Breidenstein, C. de la Fuente-Nunez, R. E. W. Hancock, *Trends Microbiol.* **2011**, *19*, 419; c) G. M. Rossolini, E. Mantengoli, *Clin. Microbiol. Infect.* **2005**, *11*, 17; d) J. A. Driscoll, S. L. Brody, M. H. Kollef, *Drugs* **2007**, *67*, 351.

[3] J. Li, R. L. Nation, J. D. Turnidge, R. W. Milne, K. Coulthard, C. R. Rayner, D. L. Paterson, *Lancet Infect. Dis.* **2006**, *6*, 589.

[4] a) M. Li, T. T. Zhang, L. F. Zhu, R. Wang, Y. G. Jin, *Int. J. Pharm.* **2017**, *528*, 163; b) Z. L. Li, D. L. Clemens, B. Y. Lee, B. J. Dillon, M. A. Horwitz, J. I. Zink, *ACS Nano* **2015**, *9*, 10778; c) Q. Y. Wang, G. J. Mi, D. Hickey, Y. A. Li, J. S. Tu, T. J. Webster, Y. Shen, *Biomaterials* **2018**, *160*, 107; d) N. L. S. Lee, K. Y. Yuen, C. R. Kumana, *JAMA* **2001**, *285*, 386.

[5] a) R. E. W. Hancock, D. P. Speert, *Drug Resist. Update.* **2000**, *3*, 247; b) S. de Bentzmann, P. Plesiat, *Environ. Microbiol.* **2011**, *13*, 1655; c) V. C. Epa, A. L. Hook, C. Chang, J. Yang, R. Langer, D. G. Anderson, P. Williams, M. C. Davies, M. R. Alexander, D. A. Winkler, *Adv. Funct. Mater.* **2014**, *24*, 2085.

[6] a) N. Sharon, H. Lis, *Science* **1989**, *246*, 227; b) Z. Y. Ong, S. J. Gao, Y. Y. Yang, *Adv. Funct. Mater.* **2013**, *23*, 3682; c) B. H. Neufeld, M. J. Neufeld, A. Lutzke, S. M. Schweickart, M. M. Reynolds, *Adv. Funct. Mater.* **2017**, *27*, 1702255.

[7] A. M. Boukerb, A. Rousset, N. Galanos, J. B. Mear, M. Thepaut, T. Grandjean, E. Gillon, S. Cecioni, C. Abderrahmen, K. Faure, D. Redelberger, E. Kipnis, R. Dessein, S. Havet, B. Darblade, S. E. Matthews, S. de Bentzmann, B. Guery, B. Cournoyer, A. Imberty, S. Vidal, *J. Med. Chem.* **2014**, *57*, 10275.

[8] a) A. Imberty, E. P. Mitchell, M. Wimmerova, *Curr. Opin. Struct. Biol.* **2005**, *15*, 525; b) E. Mitchell, C. Houles, D. Sudakevitz, M. Wimmerova, C. Gautier, S. Perez, A. M. Wu, N. Gilboa-Garber, A. Imberty, *Nat. Struct. Biol.* **2002**, *9*, 918; c) J. J. T. M. Swartjes, T. Das, S. Sharifi, G. Subbiahdoss, P. K. Sharma, B. P. Krom, H. J. Busscher, H. C. van der Mei, *Adv. Funct. Mater.* **2013**, *23*, 2843.

[9] a) R. U. Kadam, M. Bergmann, M. Hurley, D. Garg, M. Cacciarini, M. A. Swiderska, C. Nativi, M. Sattler, A. R. Smyth, P. Williams, M. Camara, A.

Stocker, T. Darbre, J. L. Reymond, *Angew. Chem. Int. Ed.* **2011**, *50*, 10631; b) H. C. Flemming, J. Wingender, *Nat. Rev. Microbiol.* **2010**, *8*, 623.

[10] R. Sommer, S. Wagner, K. Rox, A. Varrot, D. Hauck, E. C. Wamhoff, J. Schreiber, T. Ryckmans, T. Brunner, C. Rademacher, R. W. Hartmann, M. Bronstrup, A. Imberty, A. Titz, *J. Am. Chem. Soc.* **2018**, *140*, 2537.

[11] a) J. L. Jimenez Blanco, C. Ortiz Mellet, J. M. Garcia Fernandez, *Chem. Soc. Rev.* **2013**, *42*, 4518; b) C. Fasting, C. A. Schalley, M. Weber, O. Seitz, S. Hecht, B. Koksch, J. Dernedde, C. Graf, E. W. Knapp, R. Haag, *Angew. Chem. Int. Ed.* **2012**, *51*, 10472; c) M. Reynolds, M. Marradi, A. Imberty, S. Penades, S. Perez, *Chem. Eur. J.* **2012**, *18*, 4264.

[12] L. Ding, W. Cheng, X. J. Wang, S. J. Ding, H. X. Ju, *J. Am. Chem. Soc.* **2008**, *130*, 7224.

[13] a) J. Deeg, M. Axmann, J. Matic, A. Liapis, D. Depoil, J. Afrose, S. Curado, M. L. Dustin, J. P. Spatz, *Nano Lett.* **2013**, *13*, 5619; b) M. E. Ivarsson, J. C. Leroux, B. Castagner, *Angew. Chem. Int. Ed.* **2012**, *51*, 4024; c) B. Lorenz, L. A. de Cienfuegos, M. Oelkers, E. Kriemen, C. Brand, M. Stephan, E. Sunnick, D. Yuksel, V. Kalsani, K. Kumar, D. B. Werz, A. Janshoff, *J. Am. Chem. Soc.* **2012**, *134*, 3326; d) K. Lin, A. M. Kasko, *Bioconjugate Chem.* **2015**, *26*, 1504; e) D. Appelhans, B. Klajnert-Maculewicz, A. Janaszewska, J. Lazniewska, B. Voit, *Chem. Soc. Rev.* **2015**, *44*, 3968.

[14] Y. N. Wang, Y. Kotsuchibashi, Y. Liu, R. Narain, *ACS Appl. Mater. Interfaces* **2015**, *7*, 1652.

[15] a) A. Bernardi, J. Jimenez-Barbero, A. Casnati, C. De Castro, T. Darbre, F. Fieschi, J. Finne, H. Funken, K. E. Jaeger, M. Lahmann, T. K. Lindhorst, M. Marradi, P. Messner, A. Molinaro, P. V. Murphy, C. Nativi, S. Oscarson, S. Penades, F. Peri, R. J. Pieters, O. Renaudet, J. L. Reymond, B. Richichi, J. Rojo, F. Sansone, C. Schaffer, W. B. Turnbull, T. Velasco-Torrijos, S. Vidal, S. Vincent, T. Wennekes, H. Zuilhof, A. Imberty, *Chem. Soc. Rev.* **2013**, *42*, 4709; b) S. Sattin, A. Bernardi, *Trends Biotechnol.* **2016**, *34*, 483.

[16] P. Teratanatorn, R. Hoskins, T. Swift, C. W. I. Douglas, J. Shepherd, S. Rimmer, *Biomacromolecules* **2017**, *18*, 2887.

[17] a) R. Joseph, A. Naugolny, M. Feldman, I. M. Herzog, M. Fridman, Y. Cohen, *J. Am. Chem. Soc.* **2016**, *138*, 754; b) P. Zhang, S. Li, H. Chen, X. Wang, L. Liu, F. Lv, S. Wang, *ACS Appl. Mater. Interfaces* **2017**, *9*, 16933.

[18] a) R. S. Norman, J. W. Stone, A. Gole, C. J. Murphy, T. L. Sabo-Attwood, *Nano Lett.* **2008**, *8*, 302; b) S. J. Ye, G. Marston, J. R. McLaughlan, D. O. Sigle, N. Ingram, S. Freear, J. J. Baumberg, R. J. Bushby, A. F. Markham, K. Critchley, P. L. Coletta, S. D. Evans, *Adv. Funct. Mater.* **2015**, *25*, 2117.

[19] a) R. Weissleder, *Nat. Biotechnol.* **2001**, *19*, 316; b) J. V. Frangioni, *Curr. Opin. Chem. Biol.* **2003**, *7*, 626; c) S. A. Hilderbrand, R. Weissleder, *Curr. Opin. Chem. Biol.* **2010**, *14*, 71; d) R. Weissleder, V. Ntziachristos, *Nat. Med.* **2003**, *9*, 123; e) Q. Zhan, J. Qian, H. Liang, G. Somesfalean, D. Wang, S. He, Z. Zhang, S. Andersson-Engels, *ACS Nano* **2011**, *5*, 3744; f) Y. Zhong, G. Tian, Z. Gu, Y. Yang, L. Gu, Y. Zhao, Y. Ma, J. Yao, *Adv. Mater.* **2014**, *26*,

2831.
[20] a) B. Nikoobakht, M. A. El-Sayed, *Chem. Mater.* **2003**, *15*, 1957; b) L. Vigderman, E. R. Zubarev, *Chem. Mater.* **2013**, *25*, 1450.
[21] T. Masuko, A. Minami, N. Iwasaki, T. Majima, S. I. Nishimura, Y. C. Lee, *Anal. Biochem.* **2005**, *339*, 69.
[22] S. H. Kim, E. B. Kang, C. J. Jeong, S. M. Sharker, I. In, S. Y. Park, *ACS Appl. Mater. Interfaces* **2015**, *7*, 15600.
[23] A. Imberty, M. Wimmerova, E. P. Mitchell, N. Gilboa-Garber, *Microbes Infect.* **2004**, *6*, 221.
[24] J. L. Reymond, M. Bergmann, T. Darbre, *Chem. Soc. Rev.* **2013**, *42*, 4814.
[25] A. Tissieres, H. K. Mitchell, U. M. Tracy, *J. Mol. Biol.* **1974**, *84*, 389.
[26] M. J. Gething, J. Sambrook, *Nature* **1992**, *355*, 33.
[27] J. N. Rauch, E. Tse, R. Freilich, S. A. Mok, L. N. Makley, D. R. Southworth, J. E. Gestwicki, *J. Mol. Biol.* **2017**, *429*, 128.
[28] a) L. A. Dykman, N. G. Khlebtsov, *Chem. Sci.* **2017**, *8*, 1719; b) T. Bansal, R. C. Alaniz, T. K. Wood, A. Jayaraman, *Proc. Natl. Acad. Sci. U. S. A.* **2010**, *107*, 228.
[29] a) N. Aoki, K. Tateda, Y. Kikuchi, S. Kimura, C. Miyazaki, Y. Ishii, Y. Tanabe, F. Gejyo, K. Yamaguchi, *J. Antimicrob. Chemother.* **2009**, *63*, 534; b) A. Montero, J. Ariza, X. Corbella, A. Domenech, C. Cabellos, J. Ayats, F. Tubau, C. Borraz, F. Gudiol, *J. Antimicrob. Chemother.* **2004**, *54*, 1085; c) M. Labandeira-Rey, F. Couzon, S. Boisset, E. L. Brown, M. Bes, Y. Benito, E. M. Barbu, V. Vazquez, M. Hook, J. Etienne, F. Vandenesch, M. G. Bowden, *Science* **2007**, *315*, 1130.
[30] T. T. Zhang, L. F. Zhu, M. Li, Y. Z. Hu, E. F. Zhang, Q. C. Jiang, G. Han, Y. G. Jin, *Mol. Pharmaceutics* **2017**, *14*, 1718.
[31] K. Fukatsu, T. Moriya, S. Murakoshi, H. Yasuhara, *J. Surg. Res.* **2012**, *174*, 334.
[32] K. Arsalane, F. Broeckaert, B. Knoops, M. Wiedig, G. Toubeau, A. Bernard, *Am. J. Respir. Crit. Care Med.* **2000**, *161*, 1624.
[33] a) S. K. Mazmanian, J. L. Round, D. L. Kasper, *Nature* **2008**, *453*, 620; b) F. Balkwill, A. Mantovani, *Lancet* **2001**, *357*, 539; c) A. Torres, O. Sibila, M. Ferrer, E. Polverino, R. Menendez, J. Mensa, A. Gabarrús, J. Sellarés, M. I. Restrepo, A. Anzueto, M. S. Niederman, C. Agustí, *JAMA* **2015**, *313*, 677; d) B. Wonnenberg, T. Tschernig, M. Voss, M. Bischoff, C. Meier, S. H. Schirmer, F. Langer, R. Bals, C. Beisswenger, *Int. J. Med. Microbiol.* **2014**, *304*, 725; e) P. Vedak, D. Kroshinsky, J. S. John, R. J. Xavier, V. Yajnik, A. N. Ananthakrishnan, *Aliment. Pharmacol. Ther.* **2016**, *43*, 697.
[34] B. Rada, T. L. Leto, *Trends Microbiol.* **2013**, *21*, 73.
[35] C. S. Tran, Y. Eran, T. R. Ruch, D. M. Bryant, A. Datta, P. Brakeman, A. Kierbel, T. Wittmann, R. J. Metzger, K. E. Mostov, J. N. Engel, *Cell Host Microbe* **2014**, *15*, 636.

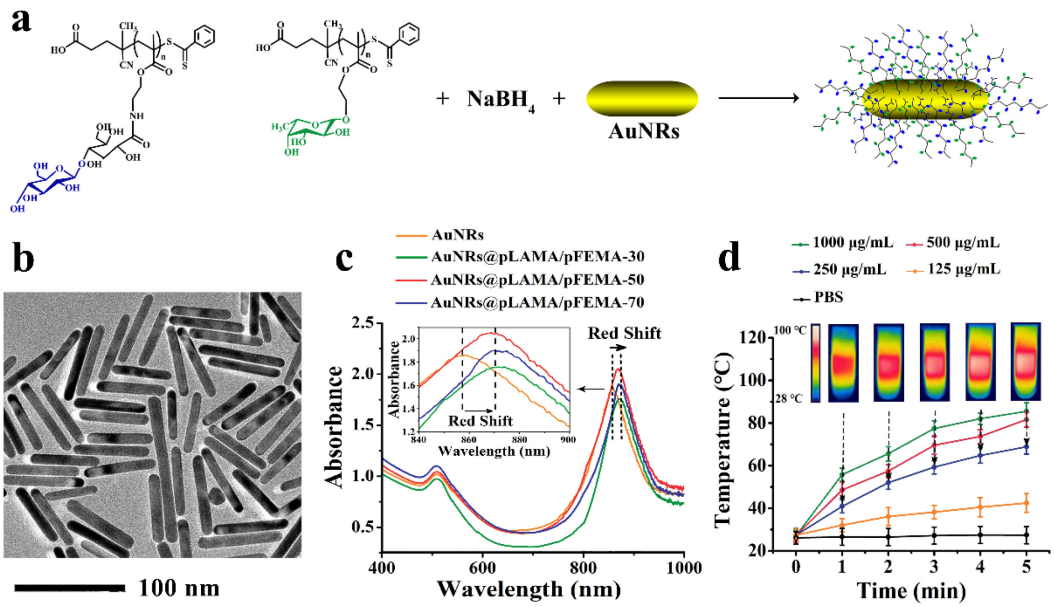

Figure 1. Fabrication and characteristics of the biomimetic nanoconjugates. a, Synthesis of AuNRs@pLAMA/pFEMA. b, TEM micrograph of AuNRs@pLAMA/pFEMA. c, UV-vis spectra of AuNRs and AuNRs@pLAMA/pFEMA. d, The temperature variation of the AuNRs@pLAMA/pFEMA solution as a function of NIR irradiation time. Insert pictures showed the thermographic images of AuNRs@pLAMA/pFEMA solution (250 μg/mL) at the end of laser irradiation.

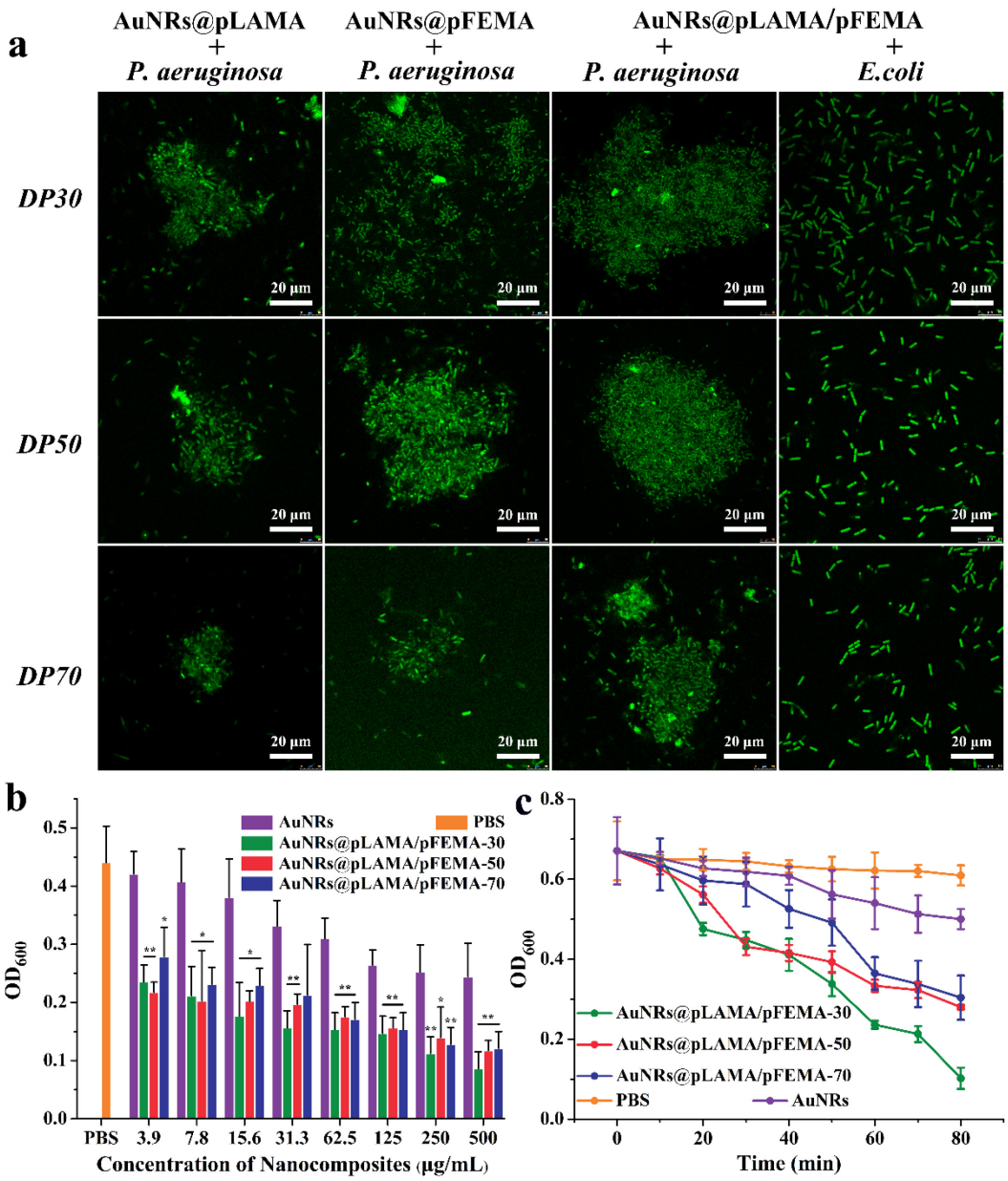

Figure 2. The interaction of the nanoconjugates with bacteria. a, CLSM images of *P. aeruginosa* and *E. coli* after incubated with AuNRs@pLAMA, AuNRs@pFEMA, and AuNRs@pLAMA/pFEMA. The OD_{600} value of the supernatant as a function with the concentration (b) and time (c) after the incubation of AuNRs@pLAMA/pFEMA nanoconjugates with *P. aeruginosa*; $*P < 0.05$, $**P < 0.01$ *vs.* AuNRs group, and all of AuNRs@pLAMA/pFEMA nanoconjugates groups showed significant different *vs.* PBS group ($P < 0.01$, not marked), one-way ANOVA with Bonferroni post hoc test.

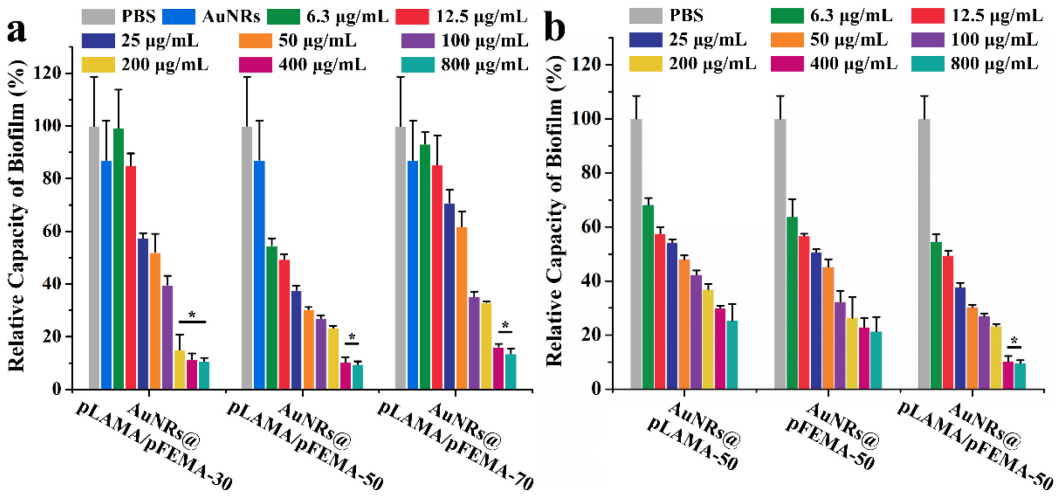

Figure 3. Inhibition of biofilm formation by the nanoconjugates. a, Inhibition of biofilm formation of AuNRs (800 μg/mL) and AuNRs@pLAMA/pFEMA containing different lengths of glycopolymer ligands, and (b) AuNRs containing different types of glycopolymer ligands. Each value represents the mean ± SD (n = 5). * $P < 0.05$, one-way ANOVA with Bonferroni post hoc test.

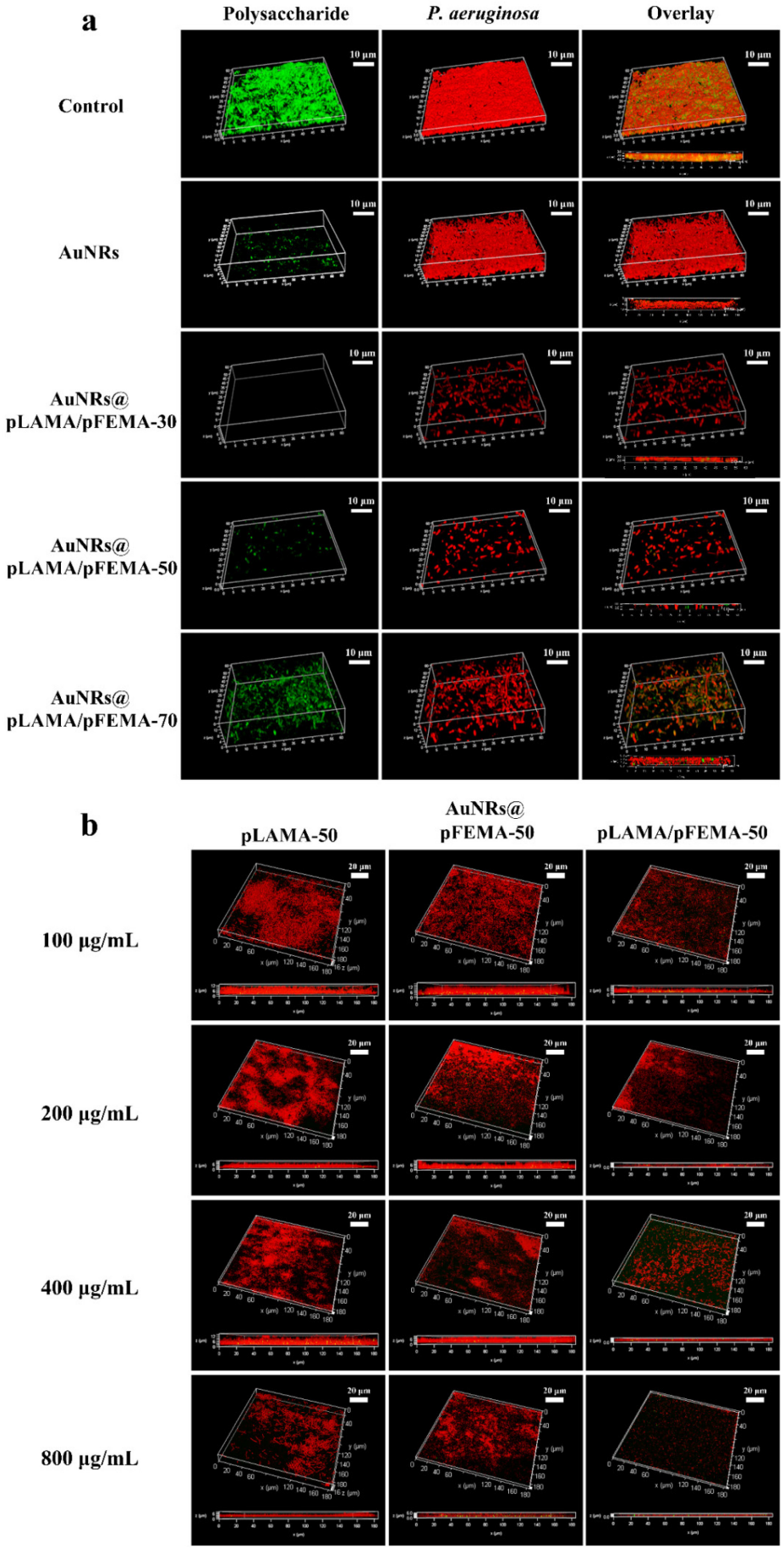
a
Polysaccharide
P. aeruginosa
Overlay
Control
AuNRs
AuNRs@ pLAMA/pFEMA-30
AuNRs@ pLAMA/pFEMA-50
AuNRs@ pLAMA/pFEMA-70
10 μm
b
pLAMA-50
AuNRs@ pFEMA-50
pLAMA/pFEMA-50
100 μg/mL
200 μg/mL
400 μg/mL
800 μg/mL
20 μm

Figure 4. CLSM images of biofilm inhibition associated with the nanoconjugates. a, *P. aeruginosa* biofilm treated without or with AuNRs and AuNRs@pLAMA/pFEMA at 200 μg/mL. b, *P. aeruginosa* biofilm treated with AuNRs@pLAMA-50, AuNRs@pFEMA-50 or AuNRs@pLAMA/pFEMA-50 at different concentrations.

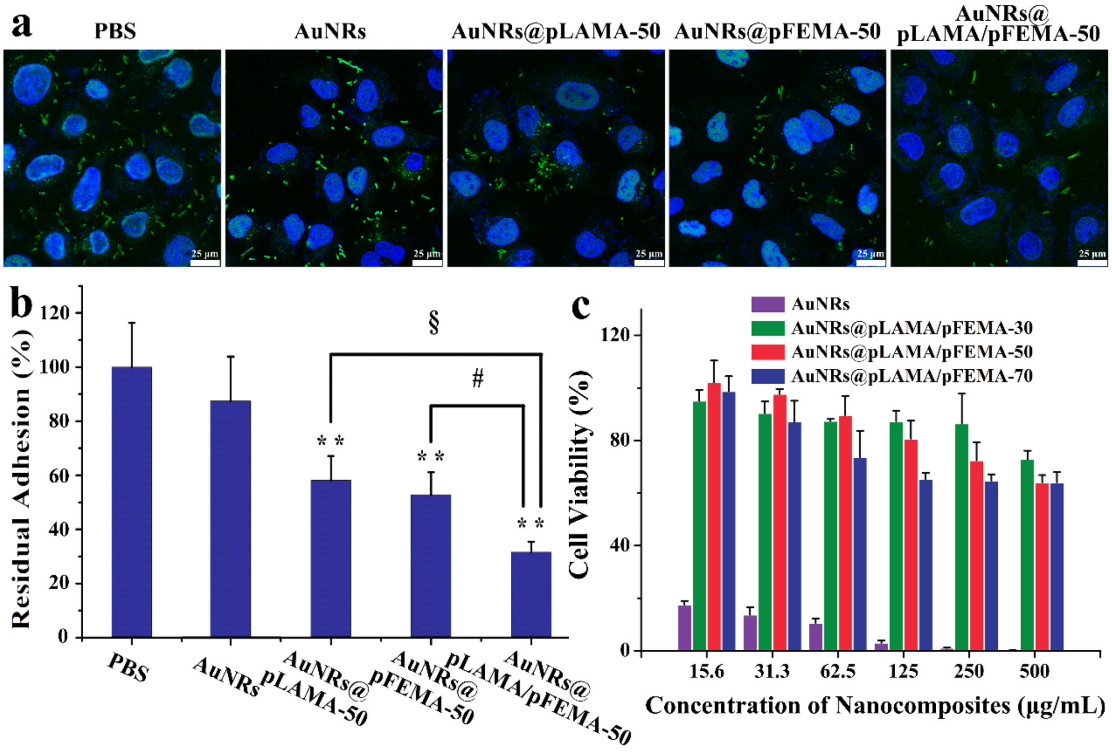

Figure 5. *In vitro* anti-adhesive activity of the nanoconjugates against *P. aeruginosa*. a, CLSM of A549 nuclei stained with DAPI, infected by *P. aeruginosa* labeled with FITC without or with the presence of AuNRs, AuNRs@pLAMA, AuNRs@pFEMA and AuNRs@pLAMA/pFEMA (100 μg/mL) after washing off non-adherent bacteria with PBS. b, Residual adhesion of *P. aeruginosa* to A549 cells after treatment with AuNRs, AuNRs@pLAMA, AuNRs@pFEMA and AuNRs@pLAMA/pFEMA at a concentration of 100 μg/mL; **P* < 0.05, ***P* < 0.01 *vs.* PBS and AuNRs group, #*P* < 0.05 *vs.* AuNRs@pLAMA group, §*P* < 0.05 *vs.* AuNRs@pFEMA group, one-way ANOVA with Bonferroni post hoc test. c, Cell viability of A549 after incubation with AuNRs@pLAMA/pFEMA for one day.

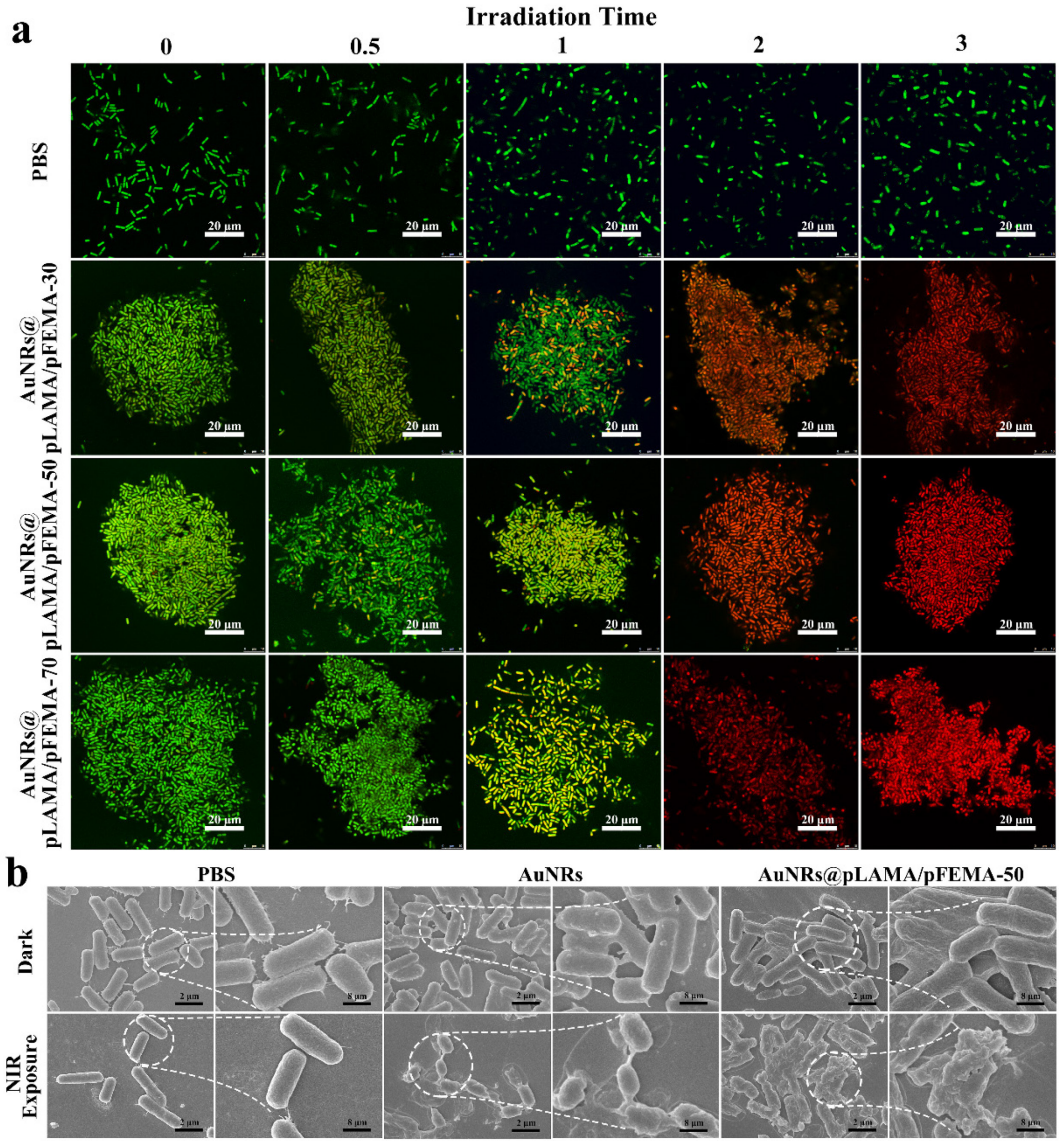

Figure 6. Photothermal lysis of *P. aeruginosa in vitro*. a, Live/Dead images of *P. aeruginosa* by CLSM after treated with AuNRs@pLAMA/pFEMA under different NIR irradiation time, stained with AO (green for live cells) and EB (red for dead cells). b, SEM images of *P. aeruginosa* after treated by PBS, AuNRs and AuNRs@pLAMA/pFEMA-50 with or without NIR laser irradiation. The control group (PBS) has no presence of AuNRs@pLAMA/pFEMA.

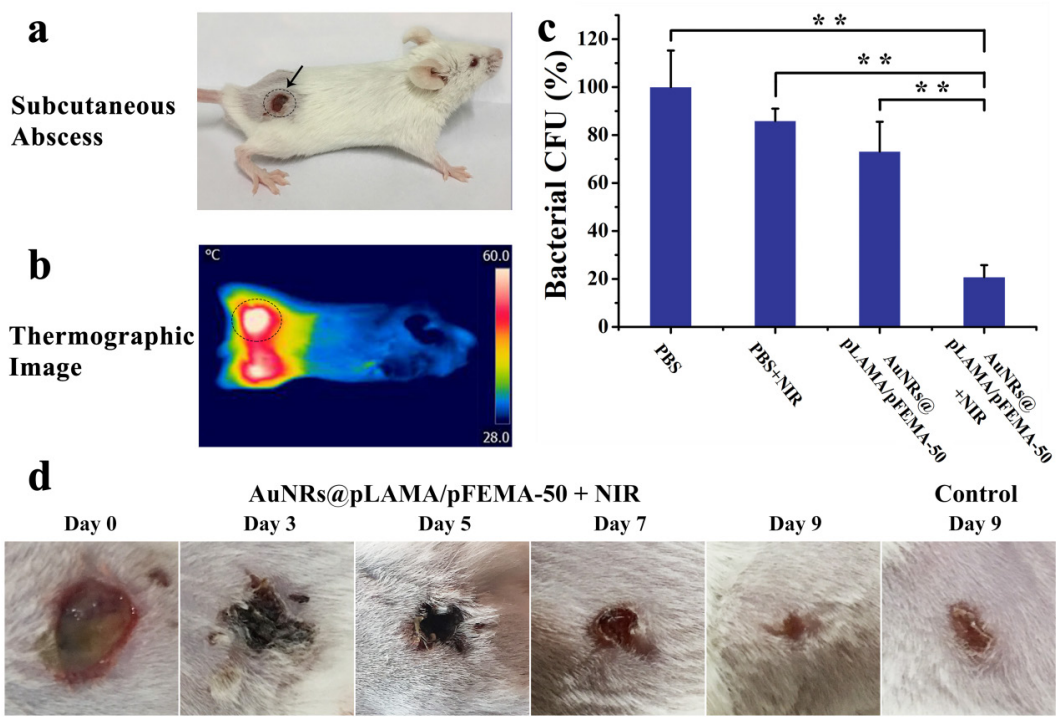

Figure 7. Photothermal therapy for focal infection *in vivo*. a, Mouse having a subcutaneous abscess developed before treatment. b, the thermographic image of mice with a subcutaneous abscess following treatment by AuNRs@pLAMA/pFEMA-50 plus NIR exposure. c, Quantitative analysis of bacterial CFU obtained from infected tissues of mice that had been treated under various experimental conditions. $^{**}P < 0.01$, one-way ANOVA with Bonferroni post hoc test. d, Photographs of the infected skin of untreated mice (day 9) and mice following the treatment of AuNRs@pLAMA/pFEMA-50 plus NIR exposure (day 0-9).

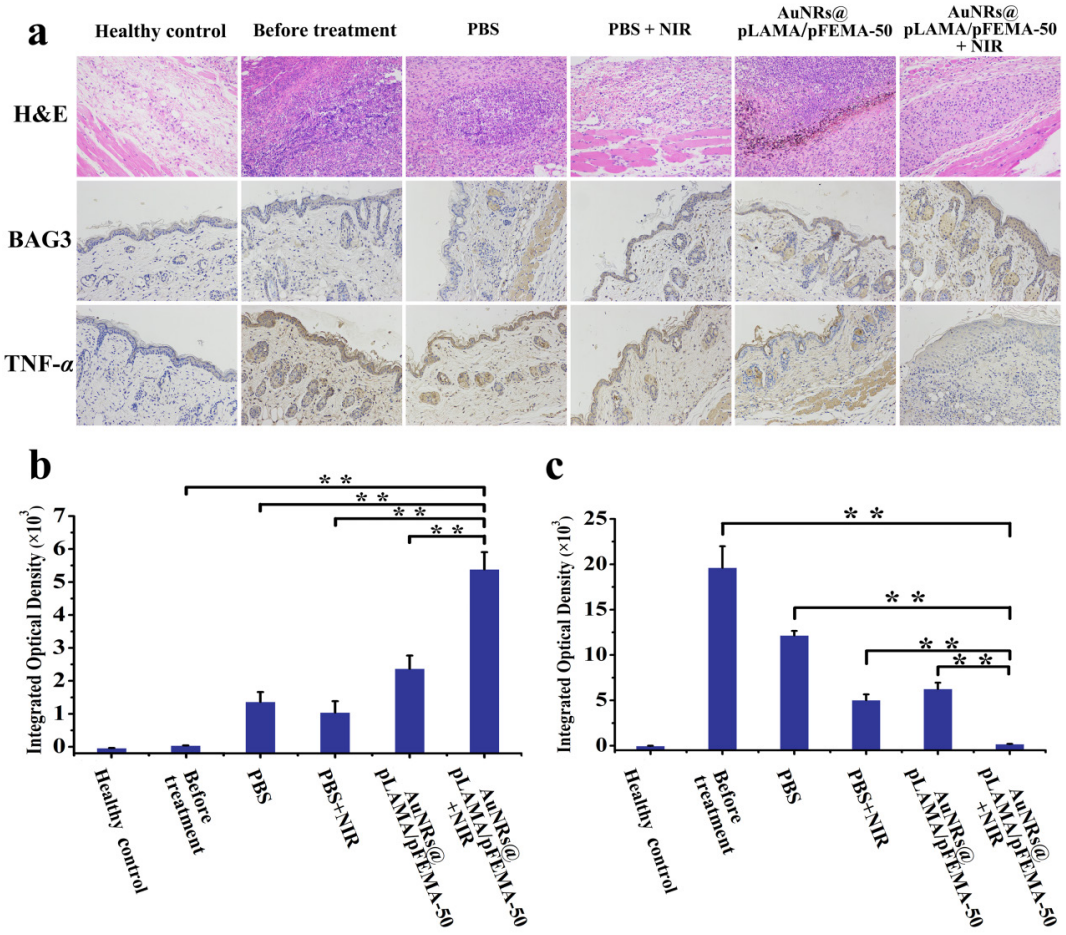

Figure 8. Inflammatory response of subcutaneous abscess after treated with the nanoconjugates. a, Histological photomicrographs of infected tissues of healthy mice, untreated mice and mice following AuNRs@pLAMA/pFEMA-50+NIR treatment after H&E staining and immunohistochemical staining of BAG3 and TNF-α. Quantitative analysis of (b) BAG3 and (c) TNF-α based on the optical density generated from the immunohistochemical staining. The infected tissues analyzed had been treated under various experimental conditions. $^{**}P < 0.01$, one-way ANOVA with Bonferroni post hoc test.

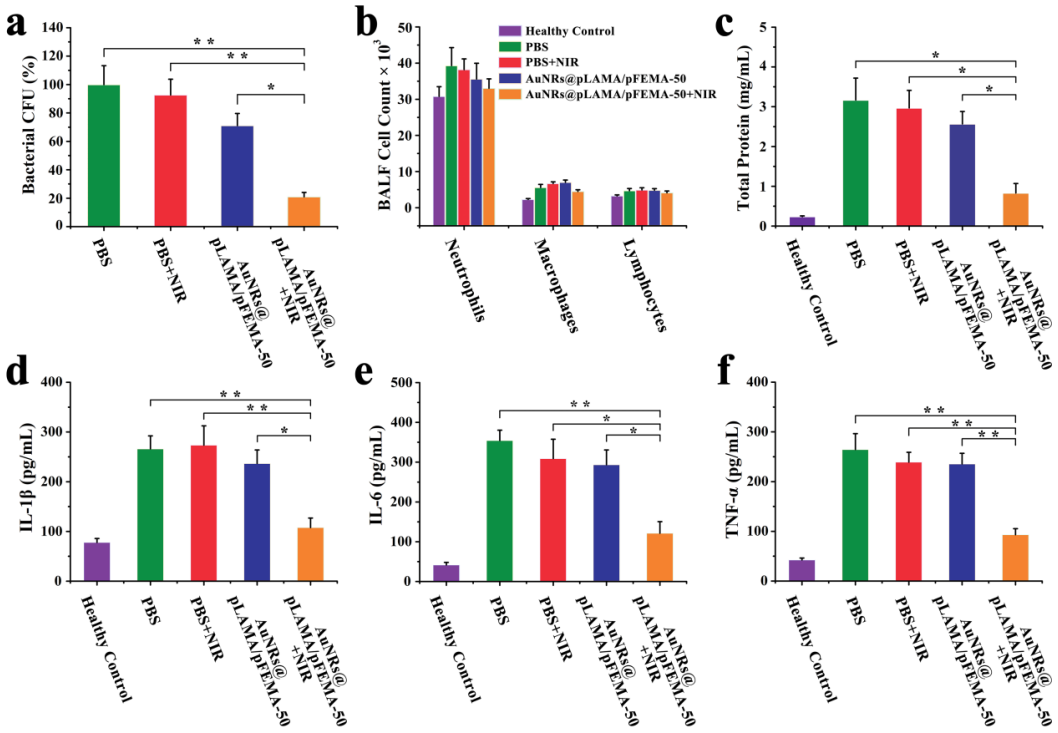

Figure 9. The inflammatory response for antibiotic-resistant bacterial pneumonia *in vivo*. Quantitative analysis of (a) bacterial CFU, (b) leukocytes, (c) total protein, (d) IL-1β, (e) IL-6 and (f) TNF-α of aminoglycoside-resistant *P. aeruginosa* induced pneumonic mice. The data were presented as mean ± SD (n = 6). *P < 0.05, **P < 0.01, one-way ANOVA with Bonferroni post hoc test.

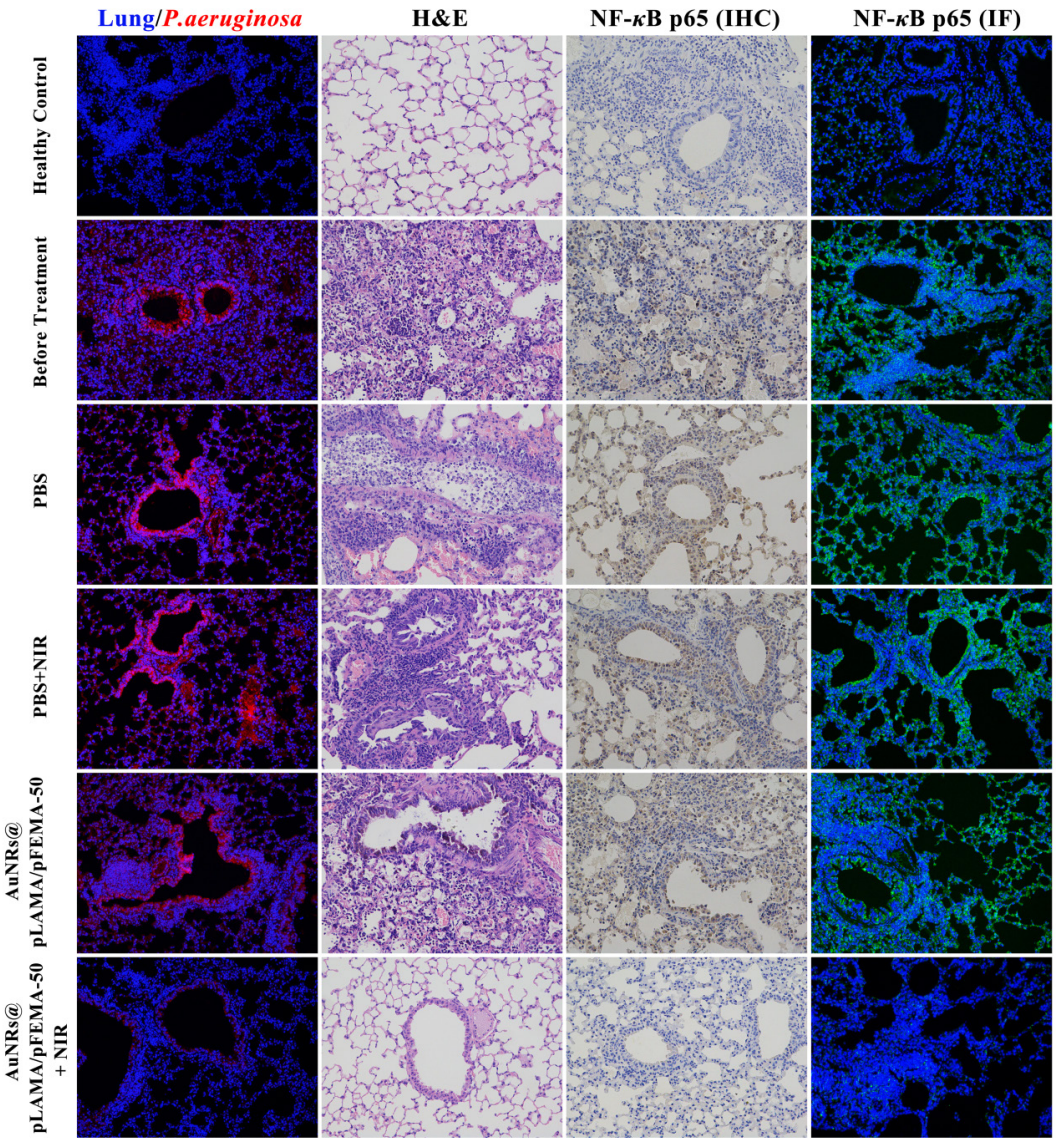

Figure 10. The suppressive inflammatory response of bronchoalveolar via the treatment of nanoconjugates. Pulmonary clearance of aminoglycoside-resistant *P. aeruginosa* by immunofluorescence analysis of lung sections, using an antibody against *P. aeruginosa*; H&E staining of lungs in each group; NF-*κ*B p65 expression in lungs by immunohistochemical and immunofluorescence staining.

Table of Content

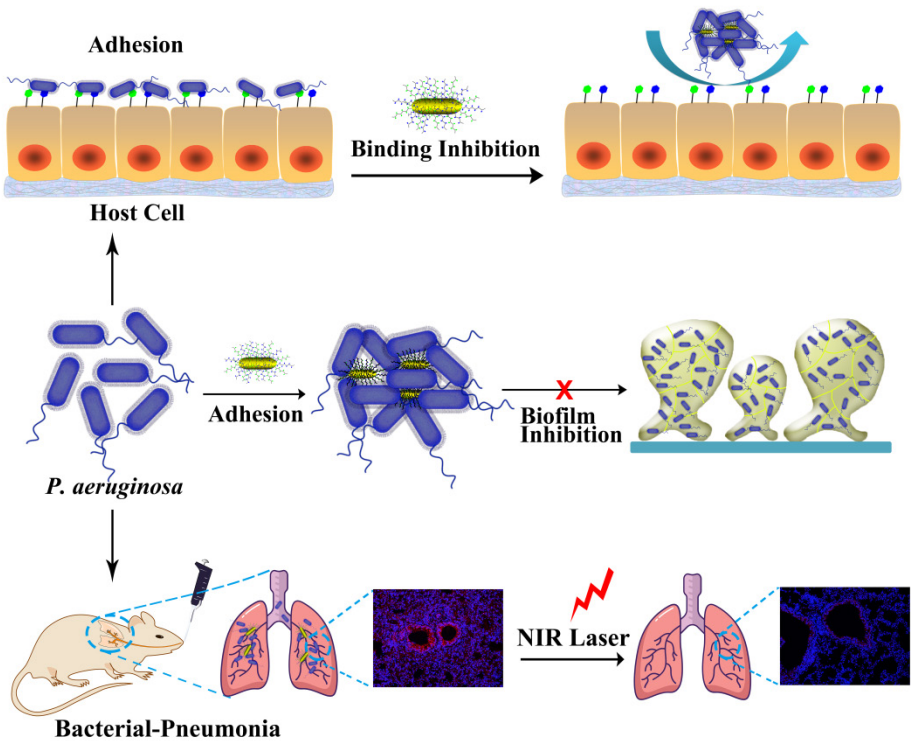

A nanoconjugate was designed to mimic natural strengthening mechanism for carbohydrate-lectin interaction occurred when bacteria initially infect the host, containing two glycomimetic ligands targeting two critical lectins of *P. aeruginosa* heteromultivalently and 3-D displayed on 50-100 nm gold nanorods. This novel formulation showed the most efficient bacteria inhibition and killing against drug-resistant *P. aeruginosa* infection, through lectin blocking and NIR induced photothermal effect, respectively.